AD-A107 684 BOLT BERANEK AND NEWMAN INC CAMBRIDGE MA F/G 20/1
BROADBAND LOW-FREQUENCY MEASUREMENT OF A DEEP-OCEAN ACOUSTIC CH--ETC(U)
AUG 81 P W SMITH, J C HEINE, A W KARP N00039-79-C-0312
UNCLASSIFIED BBN-TM-636 NL

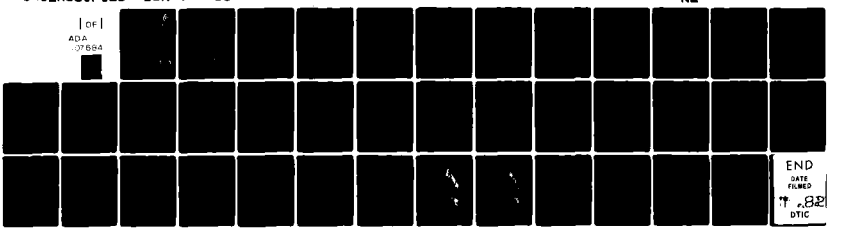

Bolt Beranek and Newman Inc.

Technical Memorandum No. 636

LEVEL II

Broadband Low-Frequency Measurement of a Deep-Ocean Acoustic Channel

P.W. Smith, Jr., J.C. Heine, and A.W. Karp

August 1981

Prepared for:
Naval Electronics Systems Command

TECHNICAL MEMORANDUM 636

BROADBAND LOW-FREQUENCY MEASUREMENT OF A DEEP-OCEAN ACOUSTIC CHANNEL

P.W. Smith, Jr., J.C. Heine and A.W. Karp

BBN Job No. 09514

Contract No.: N00039-79-C-~~0331~~ 0312

Prepared for:

Naval Electronics Systems Command
Code 612
Department of the Navy
Washington, D.C. 20360

Prepared by:

Bolt Beranek and Newman Inc.
50 Moulton Street
Cambridge, Ma. 02238

RE: Classified Reference, Distribution Unlimited.
No change in limitation per Mr. Stephen Hollis, NESC/Code 6124

TABLE OF CONTENTS

LIST OF FIGURES

LIST OF FIGURES

1. INTRODUCTION

Project DIANA, a current program at BBN under DARPA sponsorship, has as its objective the development and test of a low-frequency, impulsive-signal, active surveillance system. The October 1979 exercise was carried out in deep water west of San Francisco, near 37°N, 133°W.[1] In the course of the primary measurements, FM slides were transmitted repetitively at 8-sec intervals from a towed source, 450 ft. deep, to a towed line array, 500 ft. deep, at ranges in the neighborhood of 150 NM. The input signal frequency went from 100 to 140 Hz in 1 sec, at a constant rate; the signal amplitude was constant. The records of the received signals are the basis for the present study.

The objective of this study is to explore the feasibility of measuring appropriate fluctuation statistics of the channel, as observed in an operationally realistic situation, by coherent processing of such precisely controlled, broadband signals.

In order to design a deep ocean system (active surveillance, acoustical communications, transient detection and classification, etc.)and to predict its performance, the propagation characteristics of the channel must be understood and modelled in considerable detail. Fluctuations are particularly important to system performance; in general, a statistical model of fluctuations is called for, having only a few parameters.

Fluctuations in propagation between moving sources and receivers in the ocean have been successfully modelled as the consequence of multipath propagation in which the different paths have different depression angles and different travel times.[2-5] The result is a channel exhibiting both time- (or-range-) spread and fre-

quency- (or Doppler-) spread; its statistics can be predicted from the"scattering function" that describes these spreads of the energy of the channel's impulse response.[6] Other statistical metrics are related to these. For example, the frequency interval within which fluctuations in CW transmission are correlated ("frequency coherence interval") equals the reciprocal of the spread in travel time; it is a fundamental parameter limiting the ability to use broadband coherent processing. Similarly, the temporal coherence interval equals the reciprocal of the frequency spread.

However, the simplest such statistical model (Gaussian statistics, stationary in both frequency and space or observation time) may represent too broad-brush an average to be appropriate to some physical situations of interest. Caution is especially due in the deep ocean when the range is not very large and the range interval of interest is small as compared with the interval between convergence zones.[2,3] Several phenomena may then cause significant deviation from the simple model, especially:

i) the existence of only a small number of paths;
ii) travel-time wander, as distinct from spread;
iii) correlation between intensity variations and time spread.

The FM slides from the DIANA exercise constitute an excellent data base for examining these fluctuation questions. It is important to note that the experimental configuration -- towed source and towed line array -- is a conventional one for propagation loss experiments. However, the use of a broadband signal transmitted at a precisely controlled high repetition rate (8 sec

corresponds to 1 wavelength in range at the tow speed) results in unique advantages in comparison with conventional measurement schemes:

i) *CW Source:* yields no information on time spread or frequency coherence unless many, closely spaced frequencies are used;

ii) *Explosive Sources:* measurements are typically made at such large range intervals (exceeding 1000 wavelengths) that spatial coherence information is lost; also, variations between individual shot signatures cause an inherent loss in coherence;

iii) *Fixed Source/Fixed Receiver:* yields superior data on environmentally induced fluctuations, but no data on the operationally significant fluctuations induced by range rate.

The processing of the received signals of the DIANA exercise is briefly described here. Each ping is compressed in time by passing the signal through a matched digital filter designed from records of the source signal measured in the water. The matched-filtered signals exhibit two, well-resolved "clusters" of arrivals, in addition to noise (Fig. 1). Evidence to be described later indicates that the weaker cluster typically includes contributions from several ray paths whose travel times differ by no more than one or two resolution time intervals (1/40 Hz = 25 ms). The other stronger cluster often seems to include a single dominant path. Next, the stability of the resolved clusters is investigated. Then, in order to reduce the influence of noise, groups of 16 signals are coherently averaged. The averaged pings are further processed by (a) envelope detection and (b) spectral analysis of individual clusters.

Chapter 2 contains a theoretical discussion of the propagation in the context of simple ray theory. It is seen that the major features of the data are consistent with ray theory, although

SINGLE PING
HIGH S/N EXAMPLE

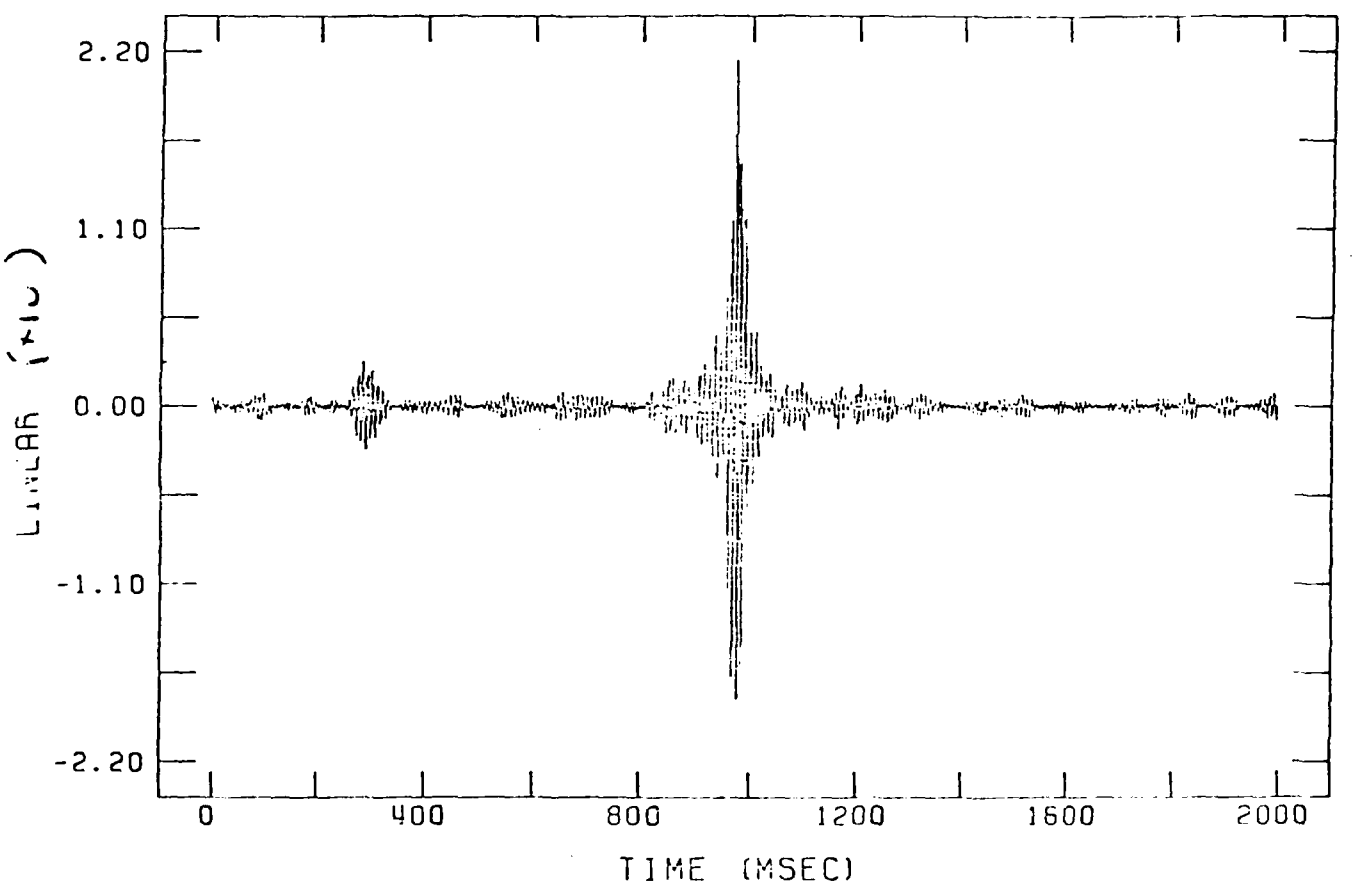

FIG. 1: SINGLE PING, AFTER MATCHED FILTERING, AT RANGE OF 150 NM

no attempt at a quantitative comparison is made.

Chapter 3 contains a discussion of measurement artifacts that may have distorted the results of the analysis. These are examples of effects that must be avoided, in advance planning, if the fluctuation statistics of the ocean transmission path alone are to be measured.

Chapter 4 presents a selection of the data and the results of analysis. The results are discussed in Chapter 5.

2. RAY-THEORY PREDICTIONS

The general features that are seen in the measured data can be predicted from ray theory. The predictions given here have been prepared from archival data for the sound speed profile. A precise numerical comparison with the measured data is not attempted but, without more precise environmental data, it probably would not indicate close agreement.

First consider the range at which a ray leaving the source at a specified D/E angle comes back to the surface; Fig. 2A shows a typical plot. In general, there is a cluster of four rays connecting the source and receiver at any range, although only one has been indicated in the figure. The four combinations of positive and negative D/E angles at both source and receiver are sensed at slightly different ranges. The differences are of the order of 1 NM in the present case, although the differences can be quite large if either the source or the receiver is deep.

At longer ranges, the rays will have made a number of cycles; the range-angle plot in the neighborhood of 150 NM is shown in Fig. 2B. Again, each curve represents a cluster of four rays. One notes that two clusters will be received: 5-cycle RSR rays with D/E angles of 12-14 deg, and 6-cycle RR rays with angles of 0-5 deg. (We accept the conventional wisdom that bottom-bounce rays will have been strongly attenuated and can be neglected.)

The strength of the signals is different for the two clusters. In ordinary ray theory, the square of signal amplitude varies directly as the slope of these curves - the reciprocal of the "range derivative".[7] Therefore, the strength will be larger for the shallow RR rays (the receiver is near a caustic) and smaller

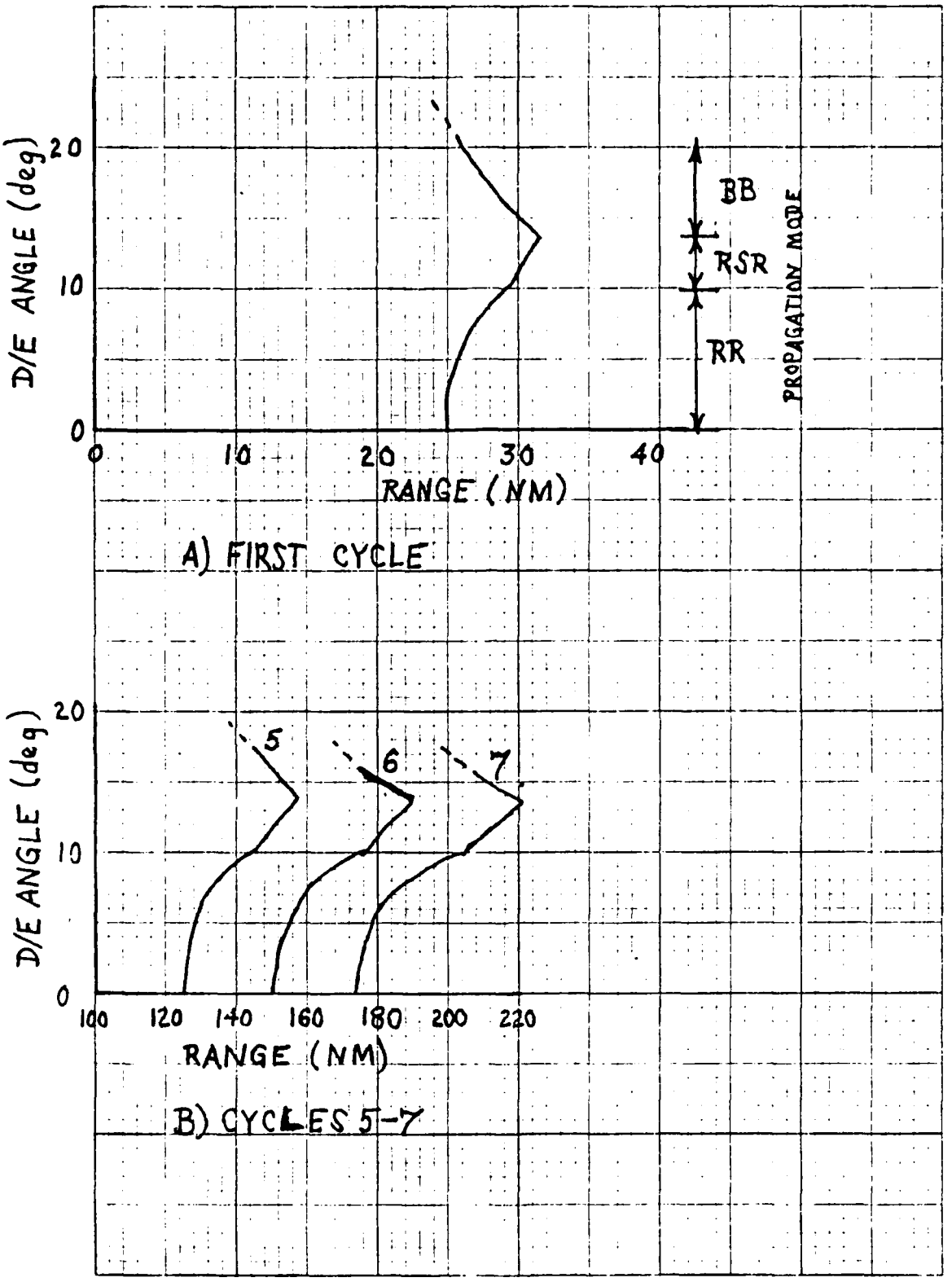

FIG. 2: TYPICAL RANGE-ANGLE PLOTS FOR SURFACE-TO-SURFACE TRANSMISSION IN THE DEEP OCEAN.

for the steeper RSR rays.

More accurate results are plotted in Fig. 3, which shows ray-theory predictions for the pressure amplitude of signal associated with each ray, plotted against the travel time.* The results for 150 NM are seen to be very similar to the measured ping in Fig. 1, when allowance is made for the fact that measurements with a 40 Hz bandwidth cannot show a "peak" narrower than 25 ms, nor resolve two peaks that are that close. The results for 154 NM are different from those for 150 NM in ways that will also be found in the measured data: the two clusters are further apart; the second cluster is weaker and more spread in time of arrival.

* Calculations were made with the Generic Sonar Model, using the Multipath Expansion Eigenray Model subroutine.[9] The program is based on generalized ray theory and includes diffracted rays as well as frequency-dependent corrections to ordinary ray theory.

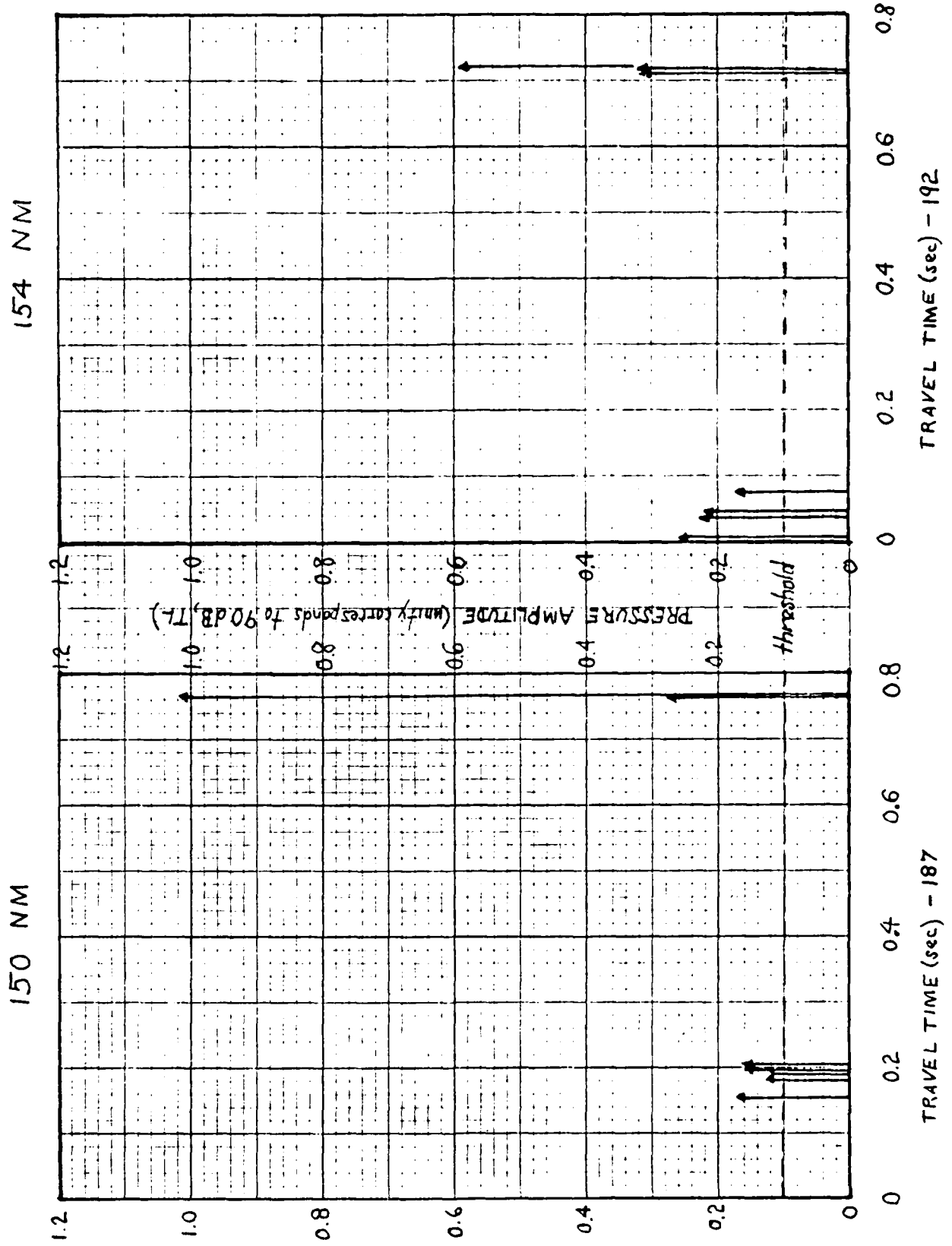

FIG. 3: TYPICAL PRESSURE AMPLITUDE-TRAVEL TIME PLOTS

3. MEASUREMENT ARTIFACTS

Several aspects of the measurement system and its operation have significantly distored the measured data, in ways that cannot be undone at this time. It is probable that both the fluctuations and the slow trends in the data have been affected. For this reason, the reduced data must *not* be taken as descriptive of the ocean transmission path alone. Any future experiment should be designed to avoid these measurement artifacts. (The plans for the 1981 exercise in Project DIANA include appropriate changes).

The measurement artifacts result from two phenomena: (1) the receiving array was not horizontal, but tilted, at an angle of 6-10 deg; (2) the array orientation fluctuated, at various time scales, to an extent that was significant with the narrow beams and the tilted array.

The effect of array tilt is most easily visualized by plotting the array sensitivity and the incident sound energy in the coordinate of *elevation angle*, measured from horizontal, and *horizontal bearing*, measured from broadside to the tow direction (Fig. 4) Then the energy of sound arriving on a single ray from a source at broadside plots as a point on the y-axis at the appropriate D/E angle. If the array were not tilted, the beam steered to broadside would be equally sensitive to energy arriving anywhere in a vertical strip including the y-axis. The strip of sensitivity is tilted when the array tilts, as shown in the figure. In the measurements, the 3-dB beamwidth was 2.2 deg at the center frequency of 120 Hz. Adjacent preformed beams near broadside were spaced at 1.5 deg. intervals.

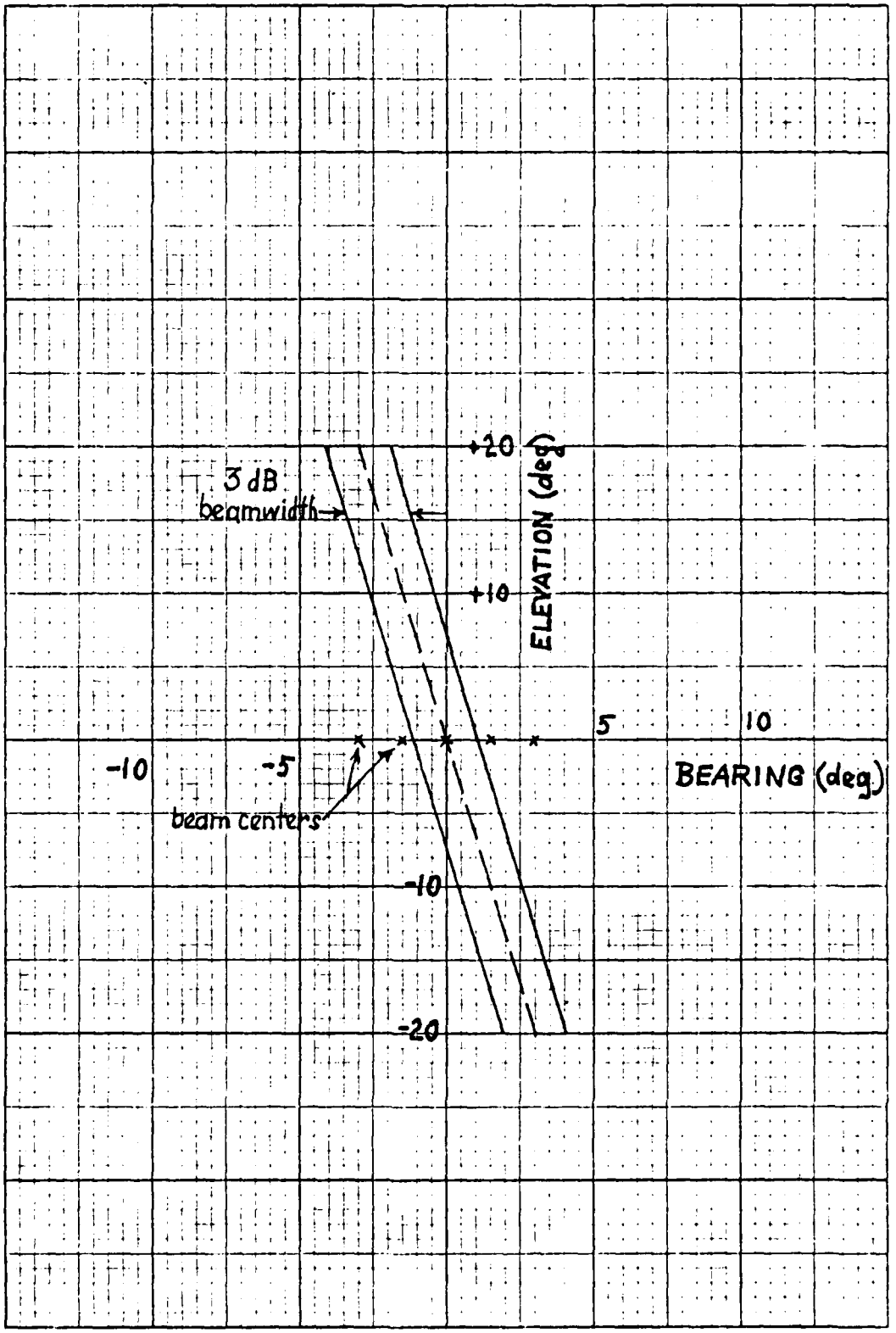

FIG. 4: SENSITIVE REGION OF A BROADSIDE BEAM OF ARRAY TILTED 8.5 DEG.

One observes from the figure that a D/E interval of only about 15 deg is included in any single beam. No single beam receives the full range of possible incidence angles, +14 to -14 deg, although at most three adjacent beams will always cover the entire range. It was the usual case in the experimental data that significant energy was seen in 3 beams.

Vertical directivity may seem a serendipitous result of tilt in a line array, until the details are examined. First, because the directive pattern of an array varies with frequency, the frequency response of the measurement system varies with the D/E angle of the incident energy. Second, the interval of D/E angle that lies in any one beam is very sensitive to small changes in the bearing of the array; angular changes are magnified by the cotangent of the tilt angle -- about 7 in the case drawn.

The effect of array motion can be inferred from fluctuations observed in the output of adjacent beams. Figures 5-7 show the evolution of the spectral levels at selected frequencies in beam 23 and its neighbors.* One notes that the signals are most intense in the center beam (no. 23), and also that they fluctuate less than those in the other two beams. (All beams show about the same secular trend with time.) It is especially significant that the fluctuations in beam -22 outputs are out of phase with those for beam 24; one goes up when the other goes down. This correlation suggests that the fluctuations are caused by a slight yawing motion of the array; the amplitude can be roughly estimated as 1/4 deg, from the level changes induced.

---

* The second, more intense cluster of ping energy was windowed and FFT'd; the squared magnitude of the outputs of the selected frequency bins were averaged over 6 pings and plotted.

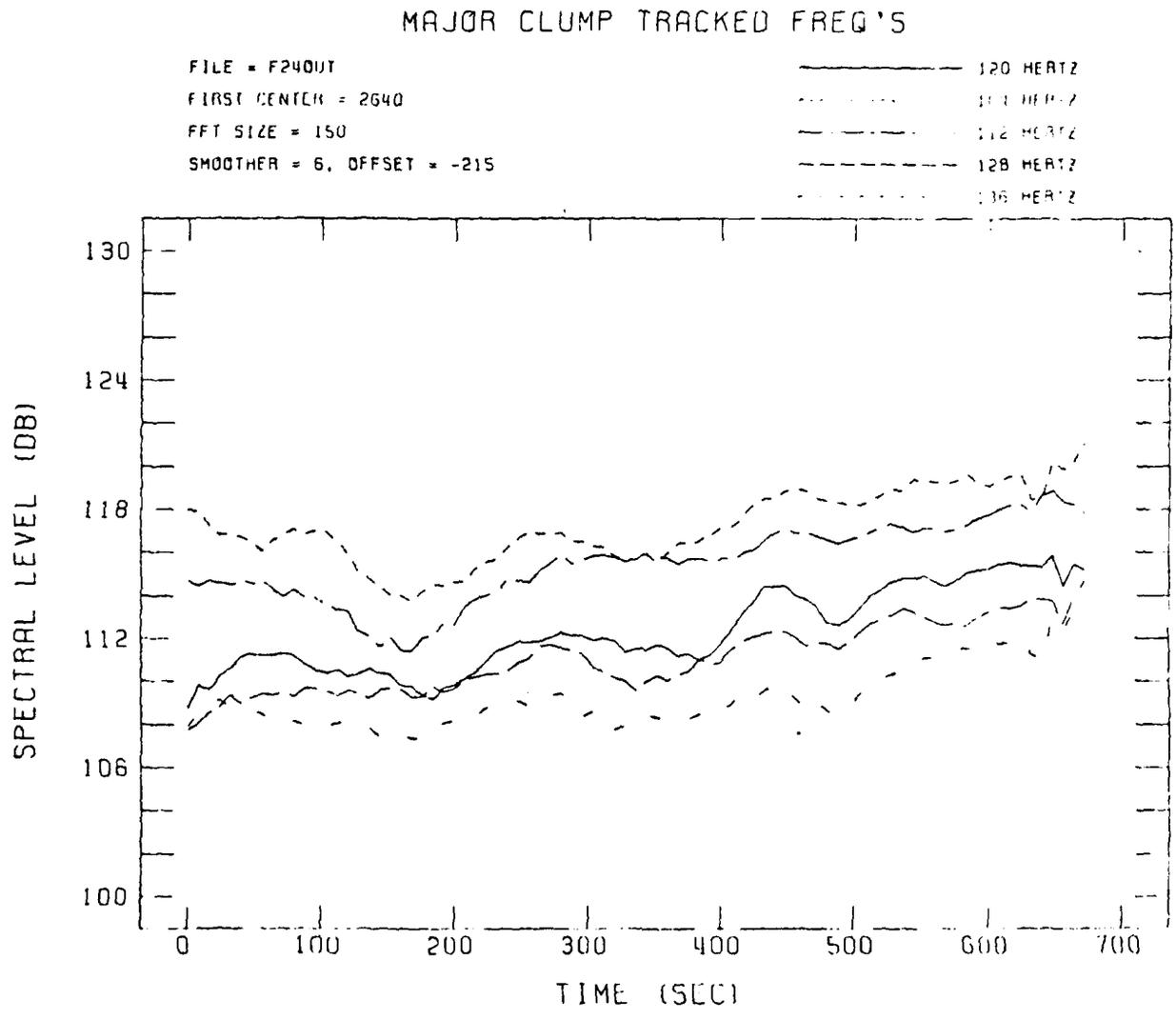

FIG. 5: LONG-TIME RECORD OF SPECTRAL LEVELS-BEAM 22

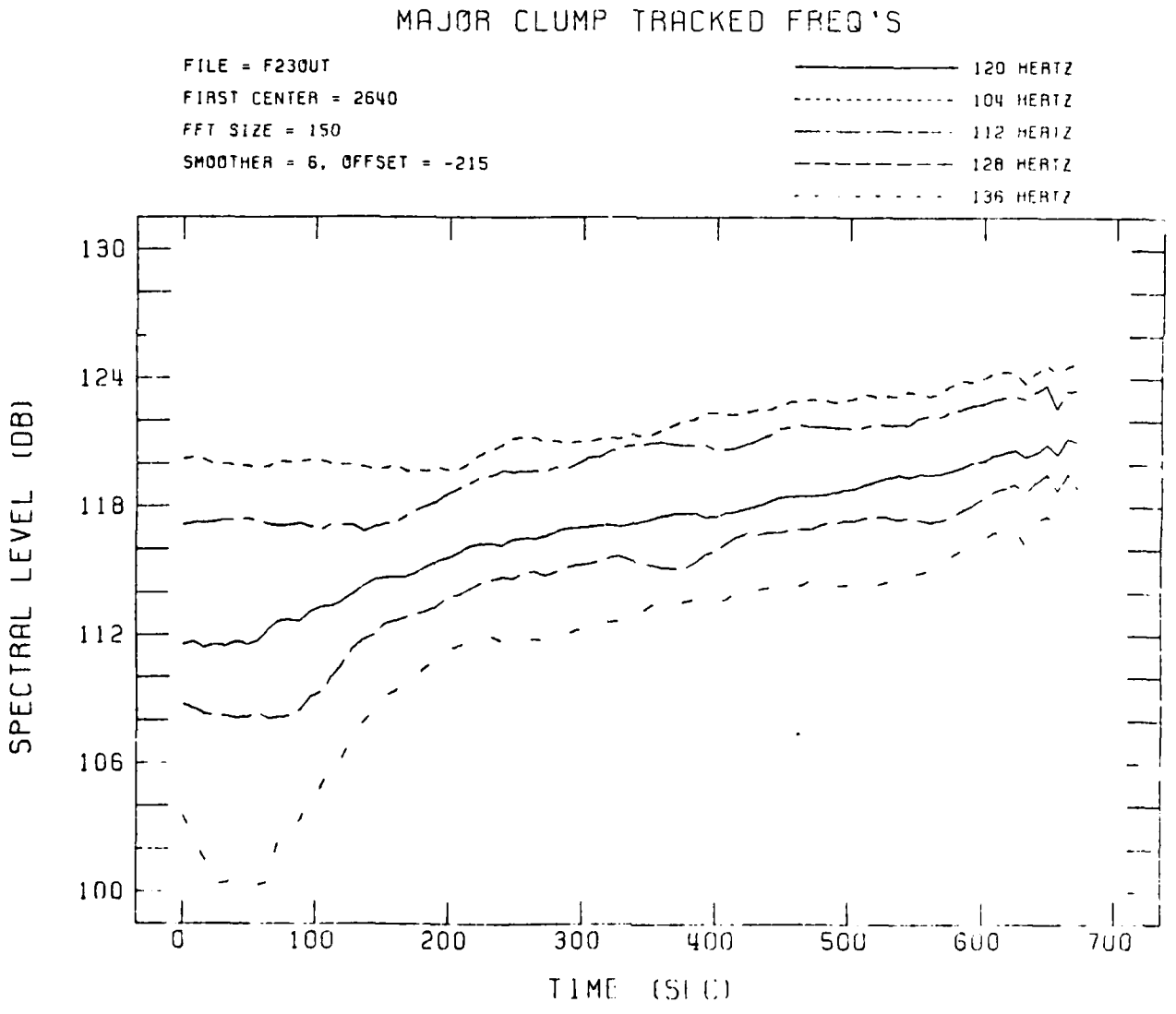

FIG. 6: LONG-TIME RECORD OF SPECTRAL LEVELS-BEAM 23

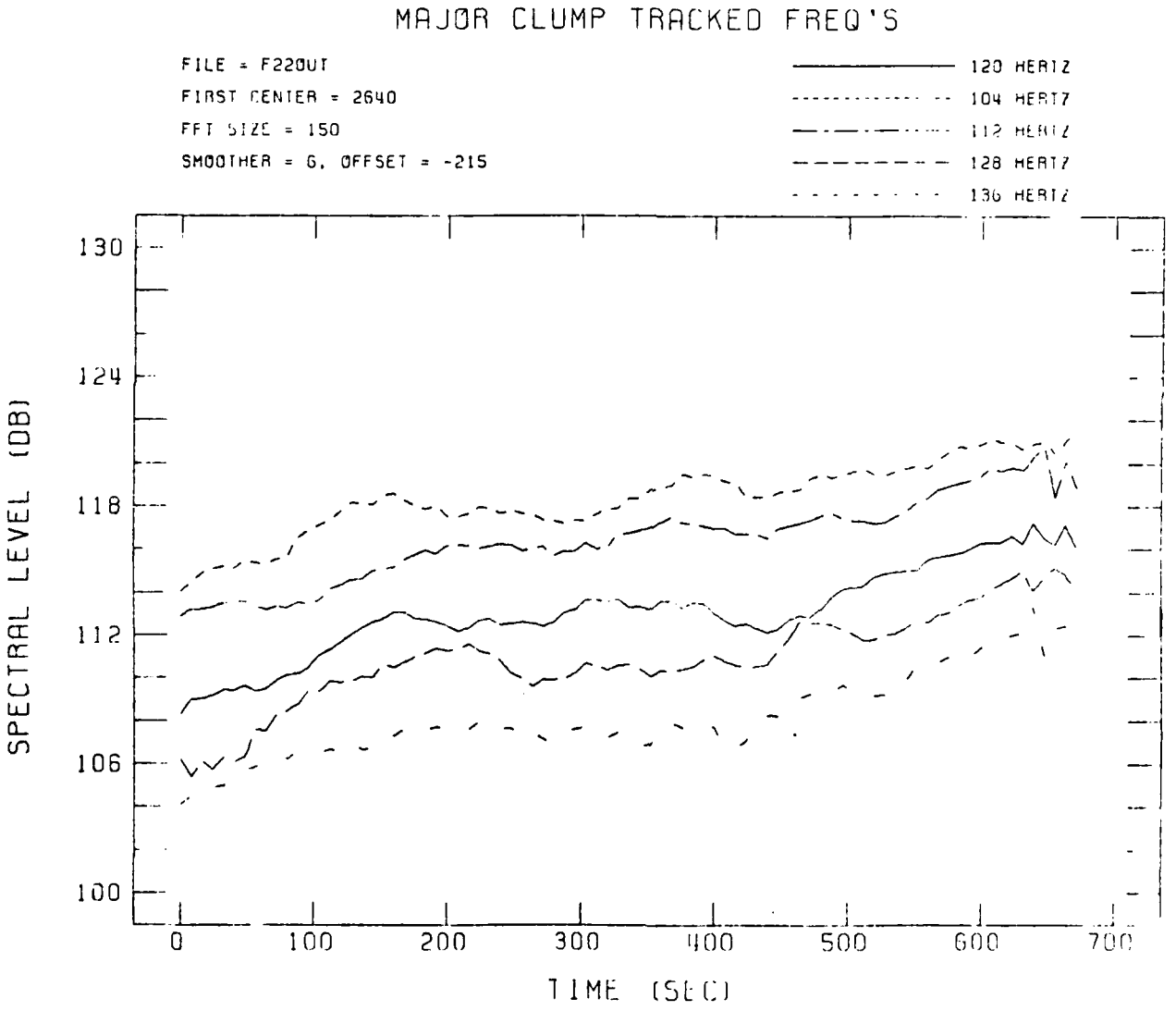

FIG. 7: LONG-TIME RECORD OF SPECTRAL LEVELS - BEAM 24

The results in Figs. 5-7 illustrate the importance of having the arriving energy centered in the measurement beam if good measurements of environmentally induced fluctuations are desired. Achievement of this goal with narrow beams (necessary in order to minimize noise) may require that the measurement beam be steered adaptively. However, even that procedure will fail to solve the problem if the array is tilted so much that no single beam can include arrivals at all D/E angles.

Only data recorded from beam 23 are used in the rest of this study. Most of the time (but not all) the signal from beam 23 was the strongest. In view of the effect of array tilt, attempts to correct for array motion were judged not to be feasible.

4. DATA REDUCTION AND RESULTS

That part of the entire data record that has been subjected to detailed analysis is about 83 min long. In this time interval the source ship closed range from about 154 to about 150 NM. The record contains about 600 pings, of which Fig. 1 is typical for records at the shorter range where the signal was stronger.

The fluctuations in the received pings are illustrated by Fig. 8. After matched filtering, a 0.5-sec sample containing the second, stronger signal cluster was FFT'd, as was a similar sample of noise alone. The outputs of the 120-Hz bin are plotted in Figs. 8-1 to 8-3 which are to be read as one continuous record. (At evident intervals, no signals were transmitted but analysis has continued, at regular 8-sec sampling intervals; these "signal" records are actually samples of noise.)

As discussed in Chapter 3, the cause of these fluctuations in level is not entirely clear; they may be, in part, measurement artifacts. Moreover, when the signal is weak (as is especially the case for the first signal cluster) noise can affect the measurements of the signal.

As a preliminary to coherent averaging of successive pings, the stability of the ping waveform was investigated. Pairs of pings were taken where the signal was well above noise; the second clusters were windowed and cross correlated. The peak value of the correlation coefficient was found to nearly equal unity for time intervals between the pings up to 16 min (Fig. 9). Another way of examining stability is shown in Fig. 10.

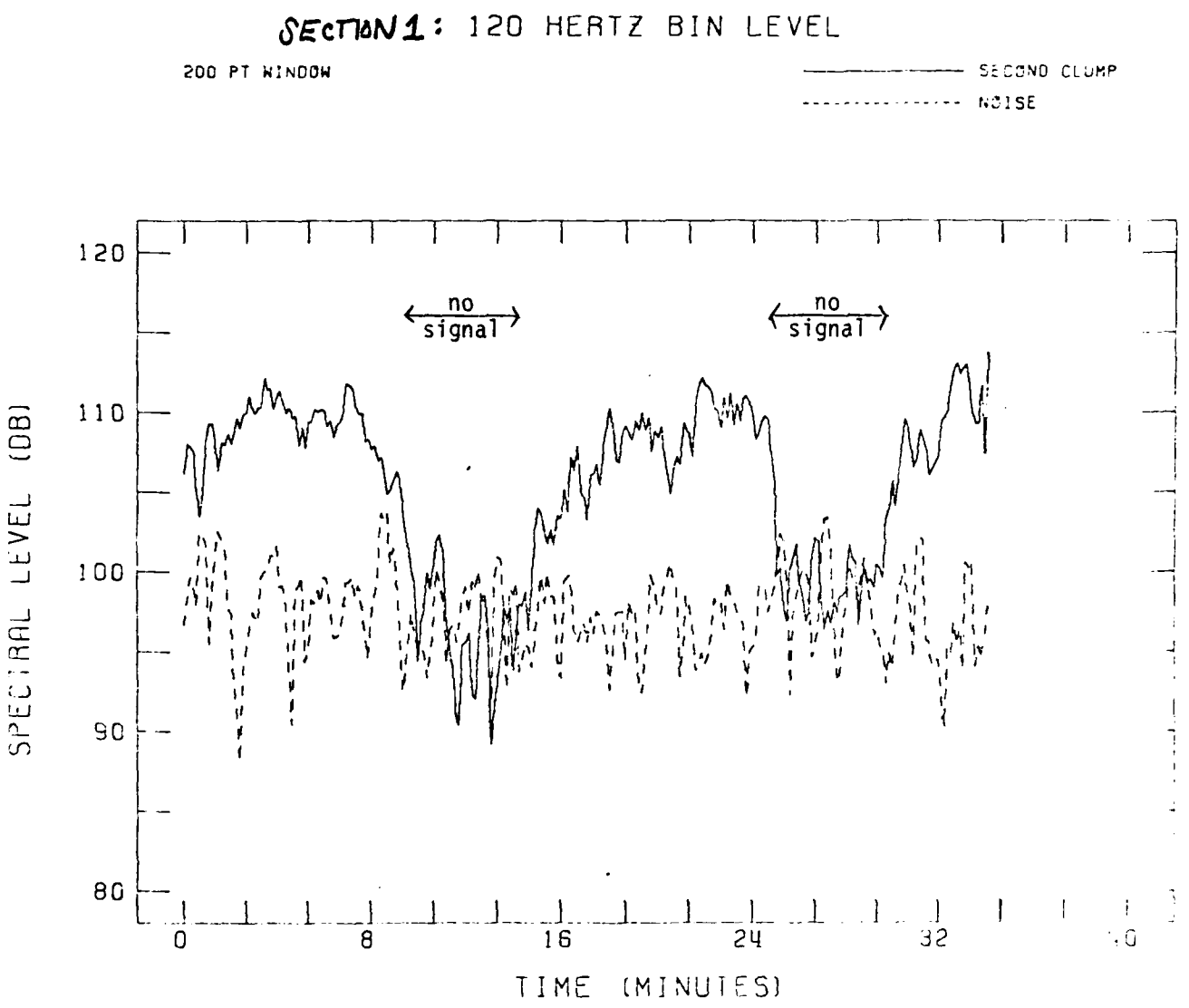

FIG. 8-1: SPECTRAL LEVELS AT 120 HZ FOR A 0.5-SEC. WINDOW CONTAINING THE SECOND SIGNAL CLUSTER (SOLID CURVE) AND A SIMILAR WINDOW OF NOISE (DASHED).

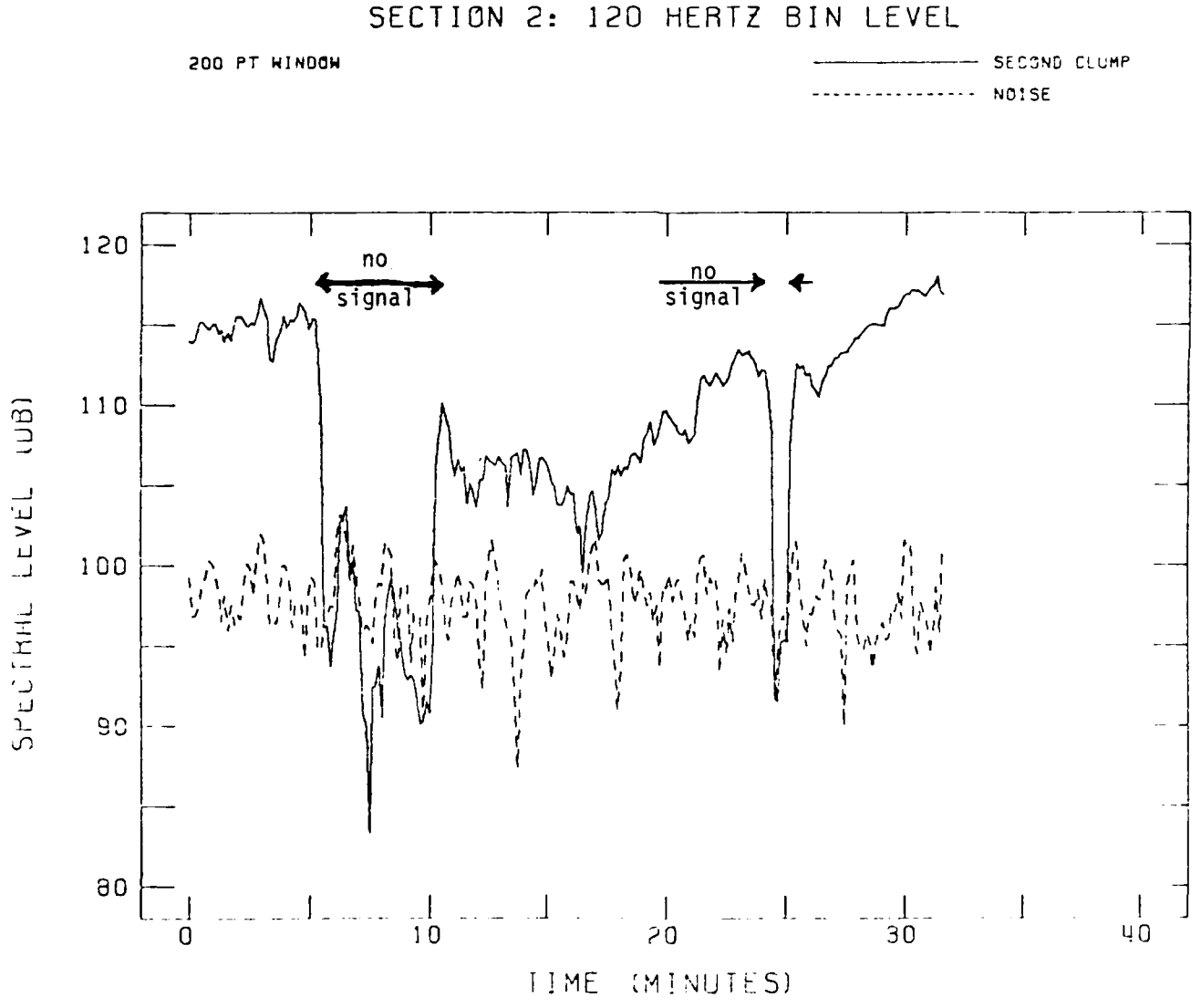

FIG. 8-2: CONTINUATION OF FIG. 8-1.

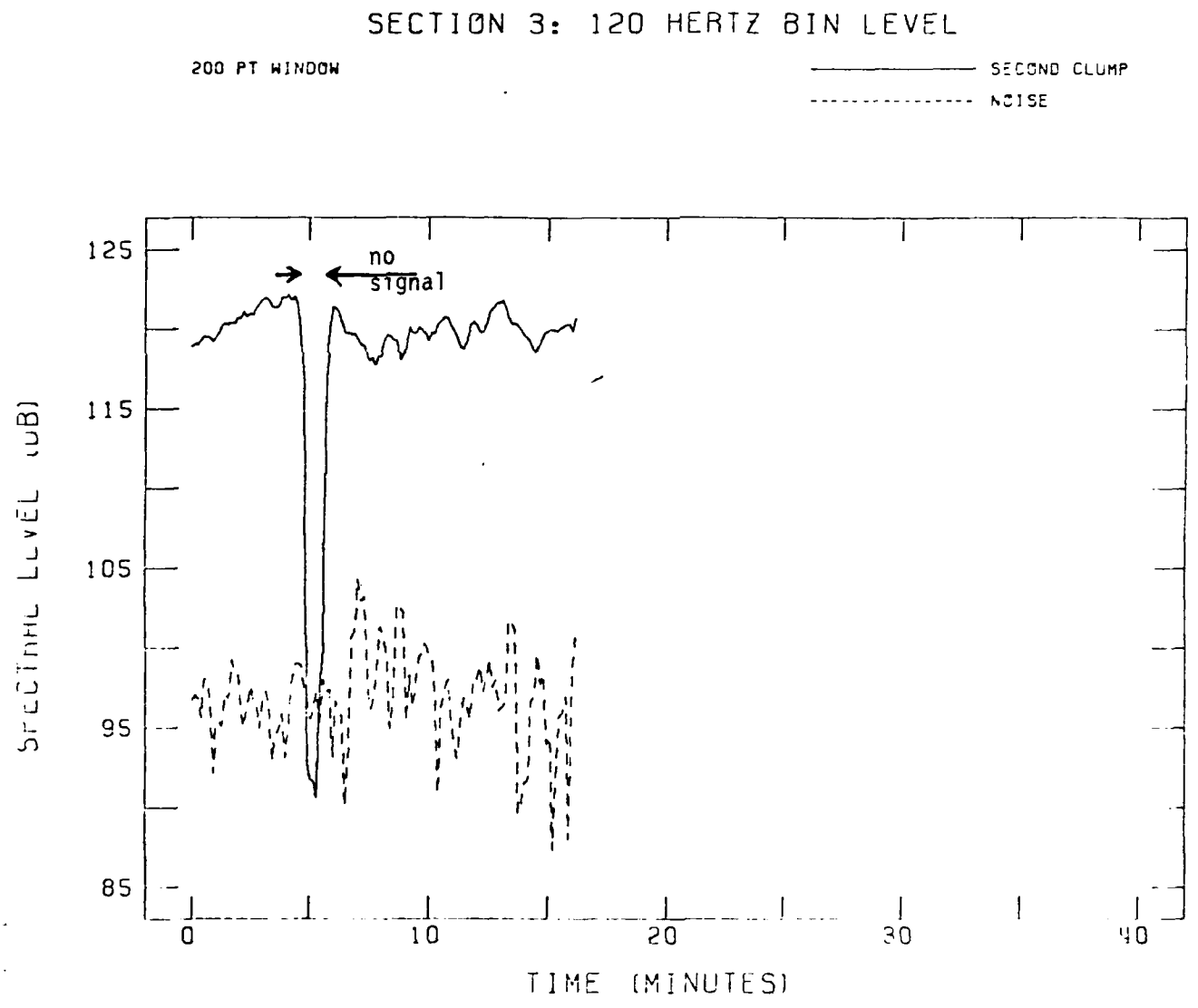

FIG. 8-3: CONTINUATION OF FIG. 8-2.

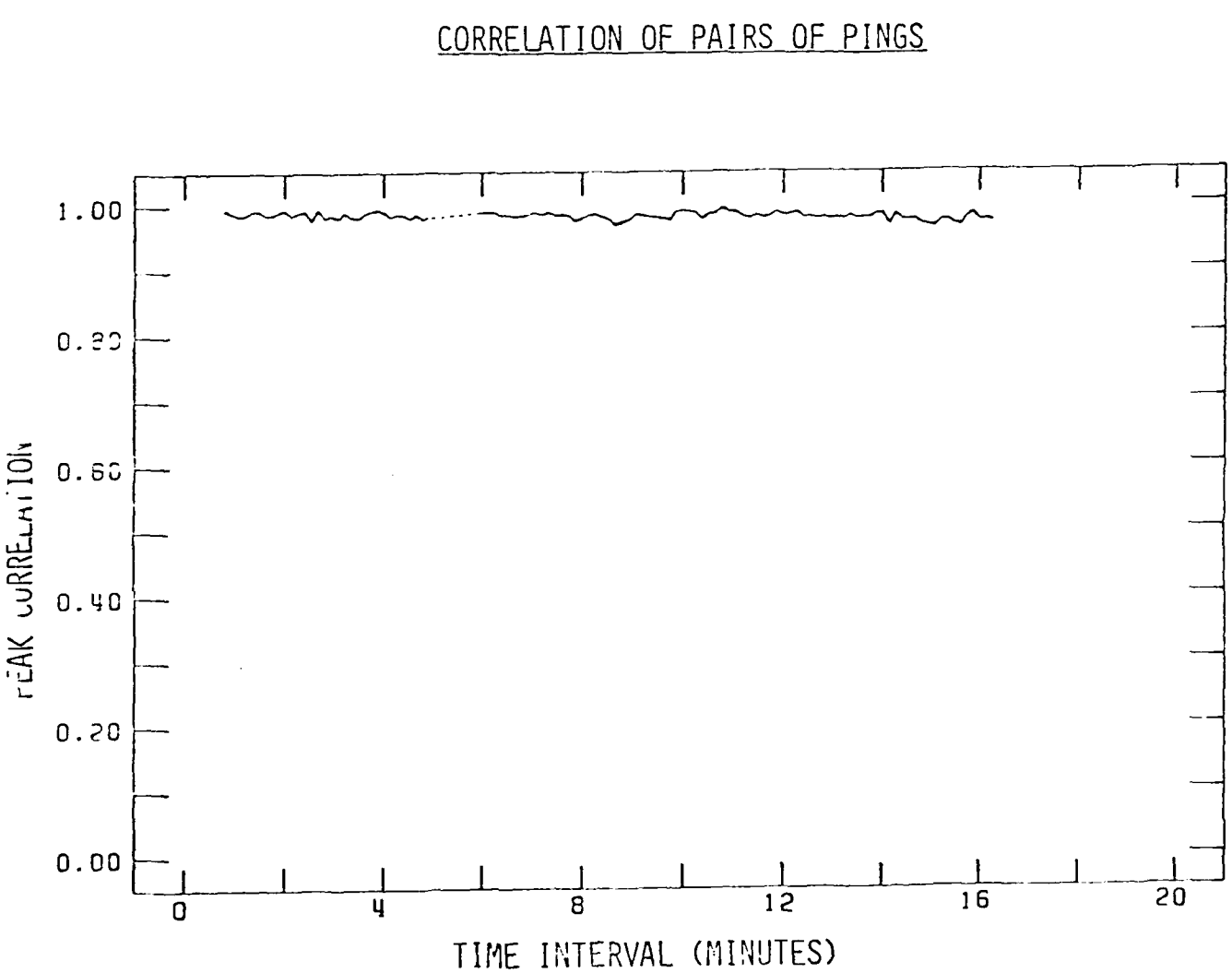

FIG. 9: PEAK VALUE OF CORRELATION COEFFICIENT FOR PAIRS OF PINGS AS FUNCTION OF TIME INTERVAL BETWEEN PINGS.

COHERENT SIGNAL GAIN DUE TO SUMMING
SUCCESSIVE PINGS

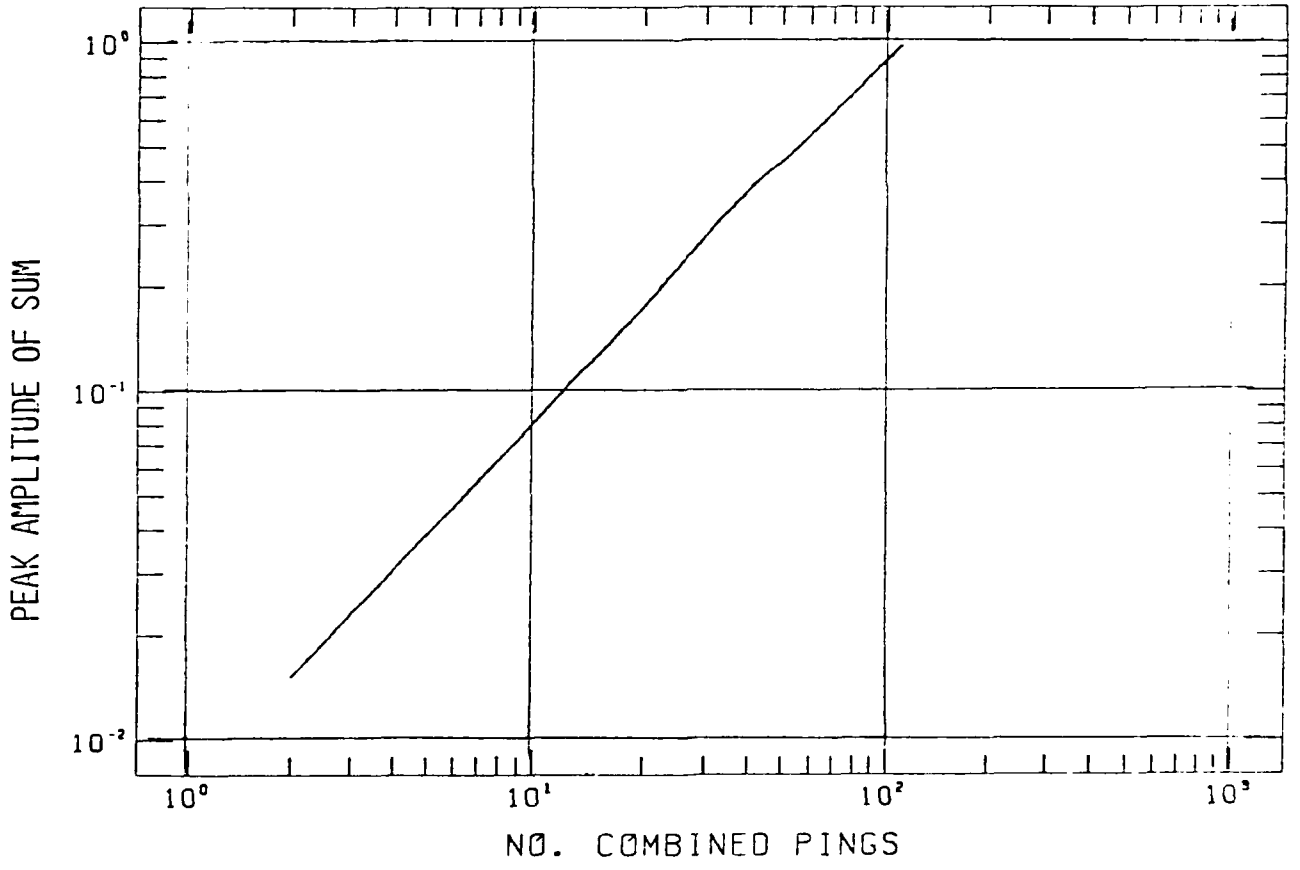

FIG. 10: THE PEAK AMPLITUDE OF THE COHERENT SUM OF N SUCCESSIVE PINGS VERSUS N.

Here the peak amplitude of the coherent sum of successive pings (second cluster) is plotted as a function of the number N of pings combined; the amplitude varies nearly linearly as N up to N = 200, corresponding to a time interval of about 27 min.

Subsequently the ping sequence was divided into groups of 16 successive pings, and the pings of each group were averaged with a time delay per ping (nominally 8 sec) that was determined by correlation. This process yielded 32 averaged pings having 12 dB (10 log 16) less noise. Figure 11-1 shows a typical averaged ping near 150 NM, where the signal is strong, while Fig. 11-2 shows an averaged ping near 154 NM where the signal is weaker. (Note the scale change; noise is essentially constant.) In addition to amplitude changes, a significant change in the time lag between clusters is observed.

The data have now been reduced to a string of 32 averaged pings, corresponding to contiguous coherent averages over a range interval of about 215 m (17 wavelengths at the center frequency). Each averaged ping contains two clusters of signal and continuous noise. Figure 12 shows the evolution of the total energy (time integral of squared signal) of each signal cluster, as well as an estimate of the power spectral density of the noise (½-sec average of squared noise divided by bandwidth, 40 Hz). Figure 13 shows the evolution of the time interval between the two clusters of signal energy, as determined by inspection. The total change (130 ms) equals about 15 periods at the center frequency of the signal.

AVERAGE OF 16 SUCCESSIVE PINGS
HIGH S/N EXAMPLE

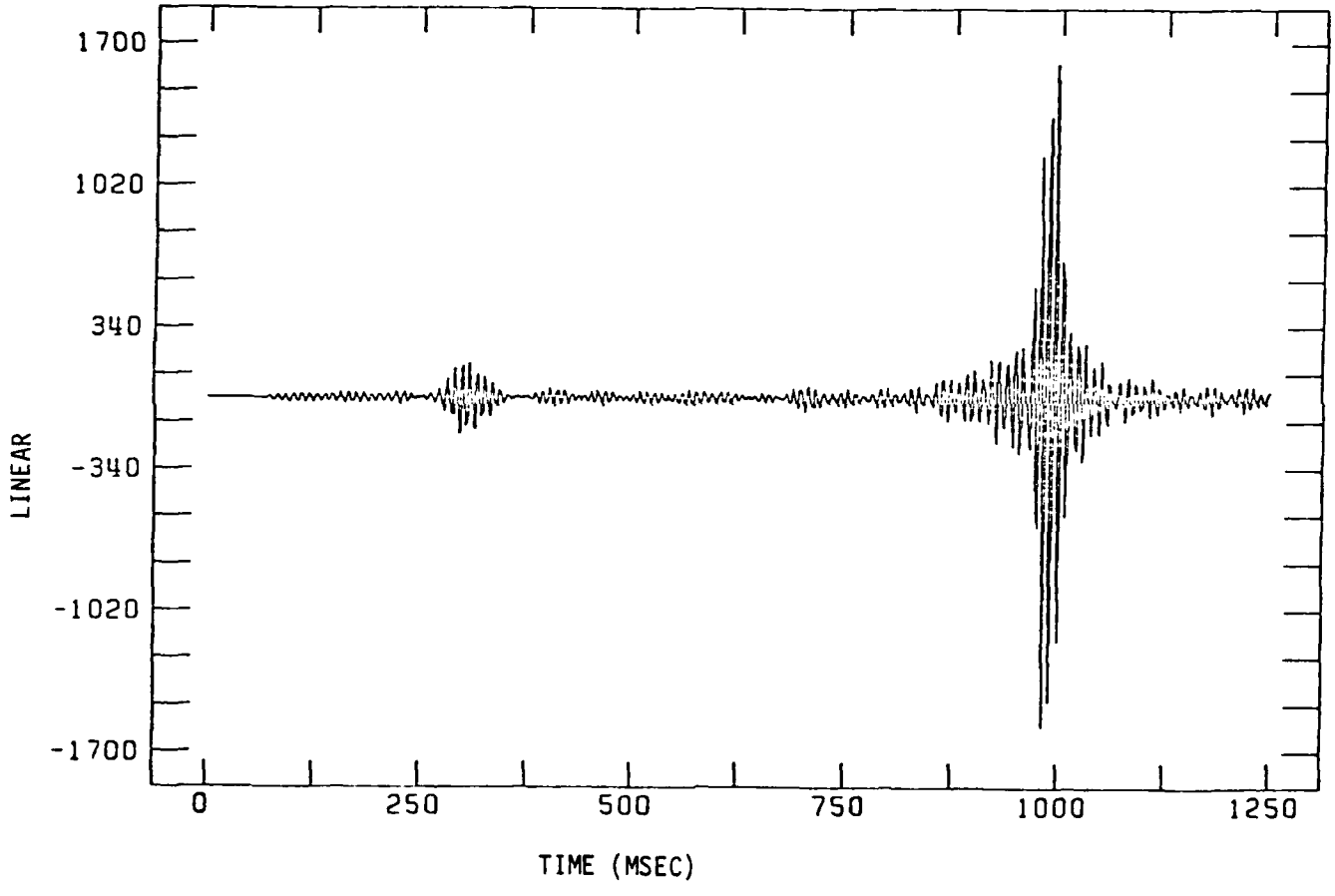

FIG. 11-1: TYPICAL AVERAGED PING AT RANGE OF ABOUT 150 NM.

AVERAGE OF 16 SUCCESSIVE PINGS
LOW S/N EXAMPLE

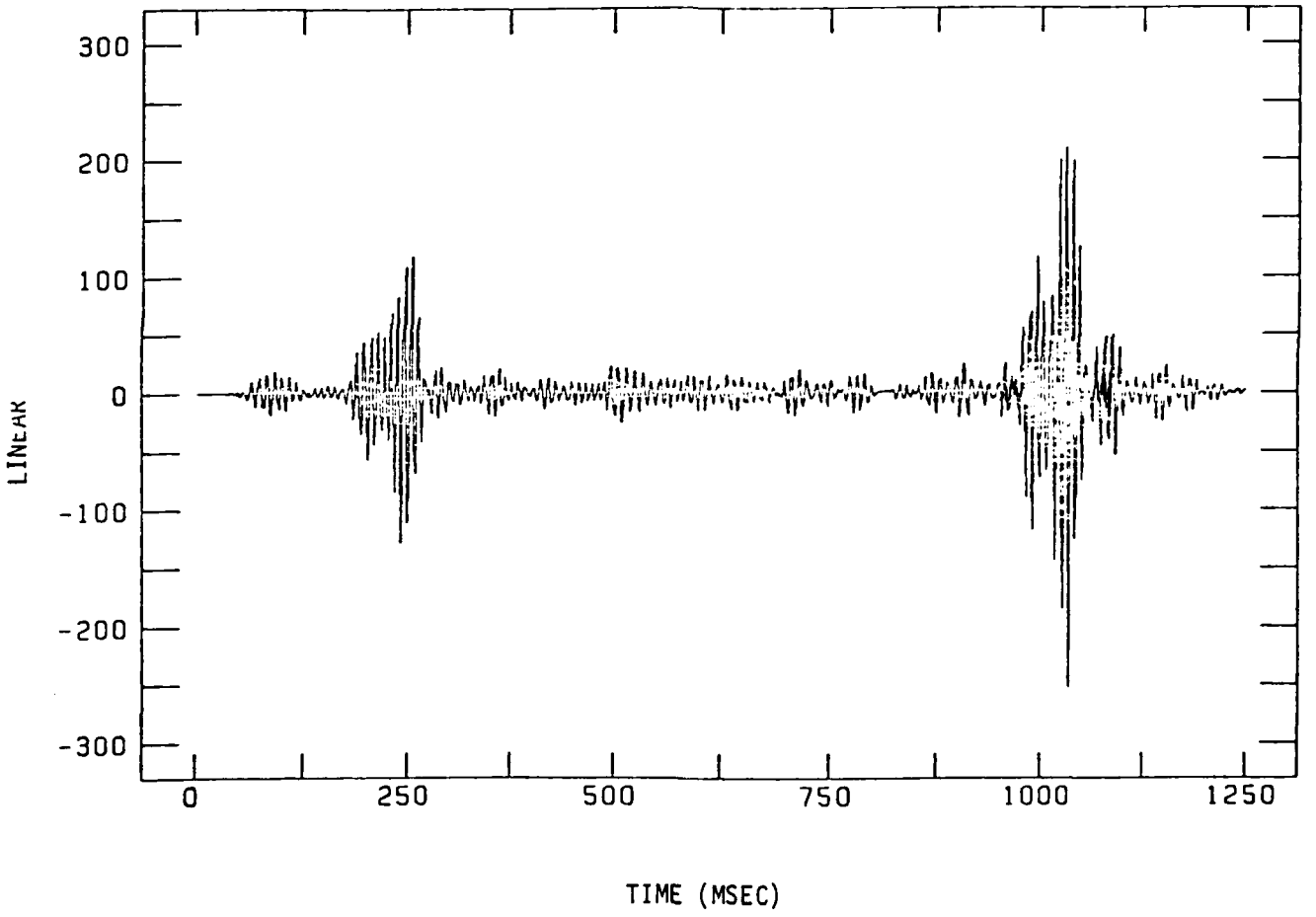

FIG. 11-2: TYPICAL AVERAGED PING AT RANGE OF ABOUT 154 NM.

LEVEL OF SIGNAL ENERGY CLUMPS AND NOISE SPECTRAL DENSITY

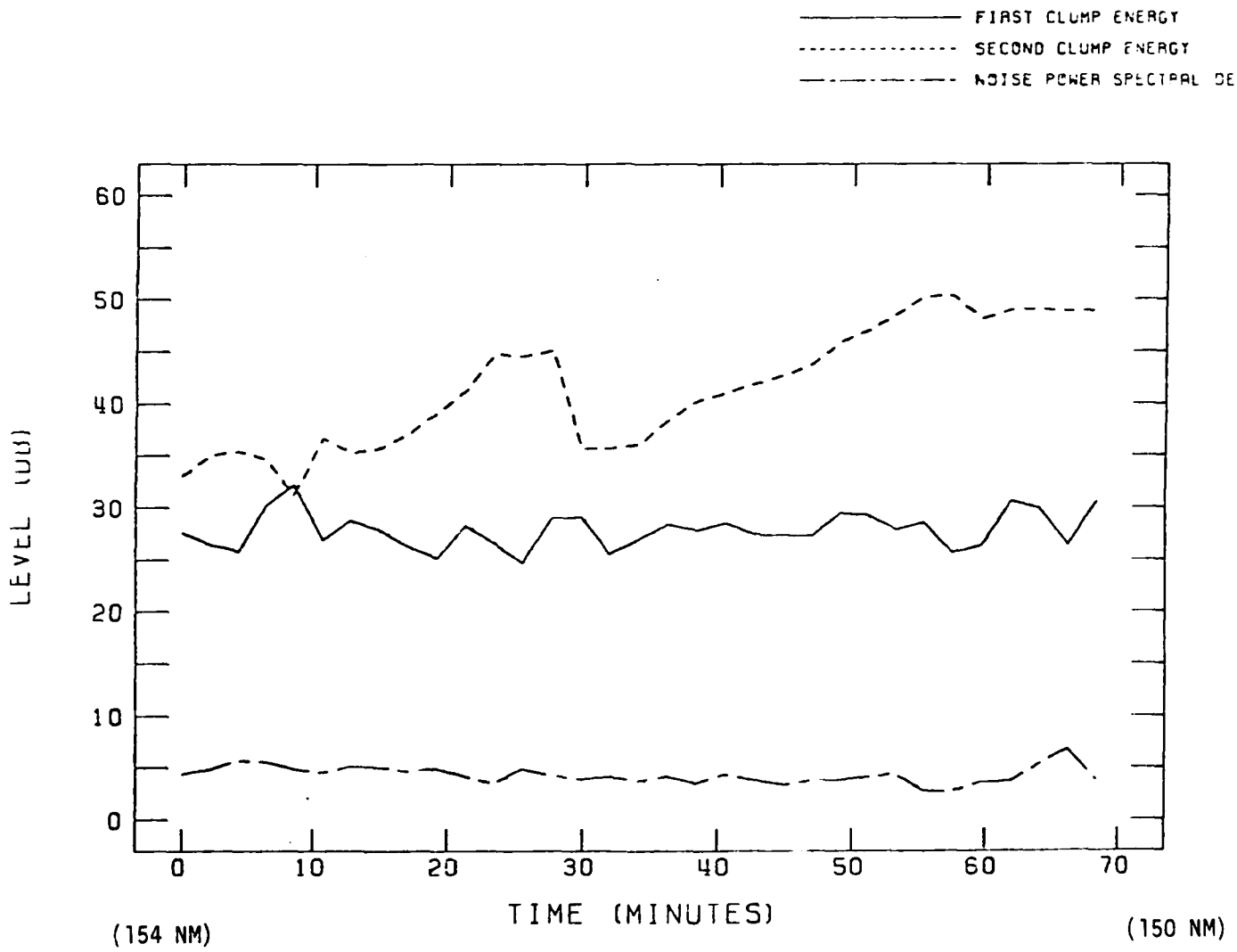

FIG. 12: ENERGY LEVEL OF THE TWO SIGNAL CLUSTERS AND SPECTRUM LEVEL OF NOISE IN AVERAGED PINGS.

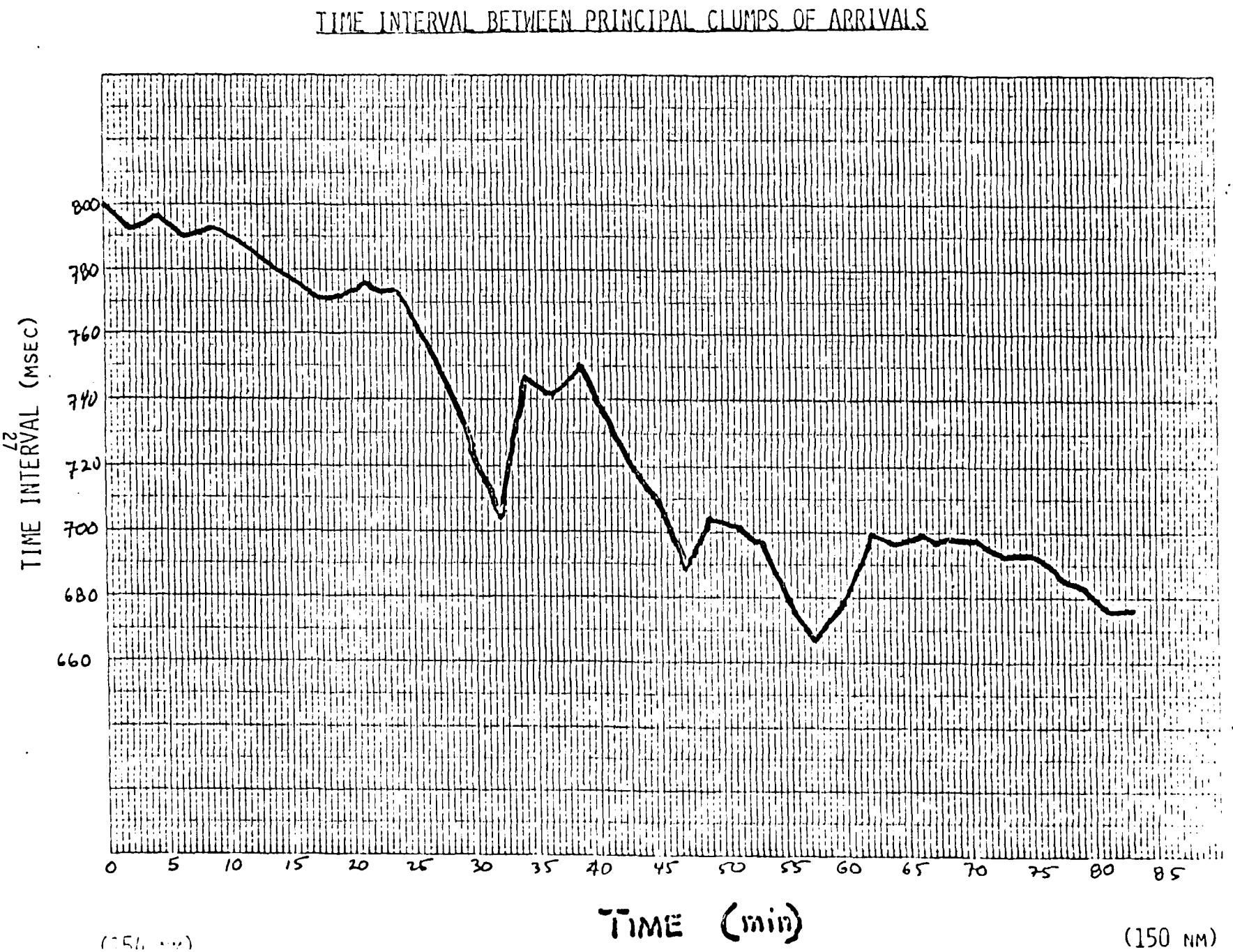

FIG. 13: TIME INTERVAL BETWEEN SIGNAL CLUSTERS

A dramatic impression of these changes is afforded by the 3-D plot of signal power level shown in Fig. 14. The individual averaged pings have been squared and smoothed by a 17.5-ms, tapered, running average. The level in dB of this "squared envelope" is shown for each of the 32 averaged pings. Noise is below the plotting threshold.

Figure 15 is a similar 3-D plot showing the evolution of the spectrum levels of the two signal clusters, obtained by FFT-ing a 375-ms sample of the averaged ping. The spectrum of the stronger, second cluster (Fig. 15-1) is somewhat irregular at first, when the energy is smaller (compare Fig. 12). At the end of the sequence, when the energy is larger (range, 150 NM), the spectrum is essentially flat, a good replica of the spectrum of the FM slide. On the other hand, the spectrum of the weaker, first cluster (Fig. 15-2) is irregular at all times.

Simple mathematical considerations indicate that the observed spectral irregularity is not here due to noise contamination of the signal in these averaged pings, although it would have been if similar processing had been applied to the pings before averaging. The most likely cause of this observed spectral irregularity is interference between several unresolved arrivals in the signal cluster.

The magnitude of noise induced fluctuations can be estimated as follows. The hypothesis we wish to reject is that the signal is due to a single arrival, so having an essentially flat spectrum, but that the measurement is contaminated by the addition of zero-mean noise. In this case, the output of a fourier transform of signal plus a sample of noise is a random complex phasor whose value is determined by signal alone. On the assumption

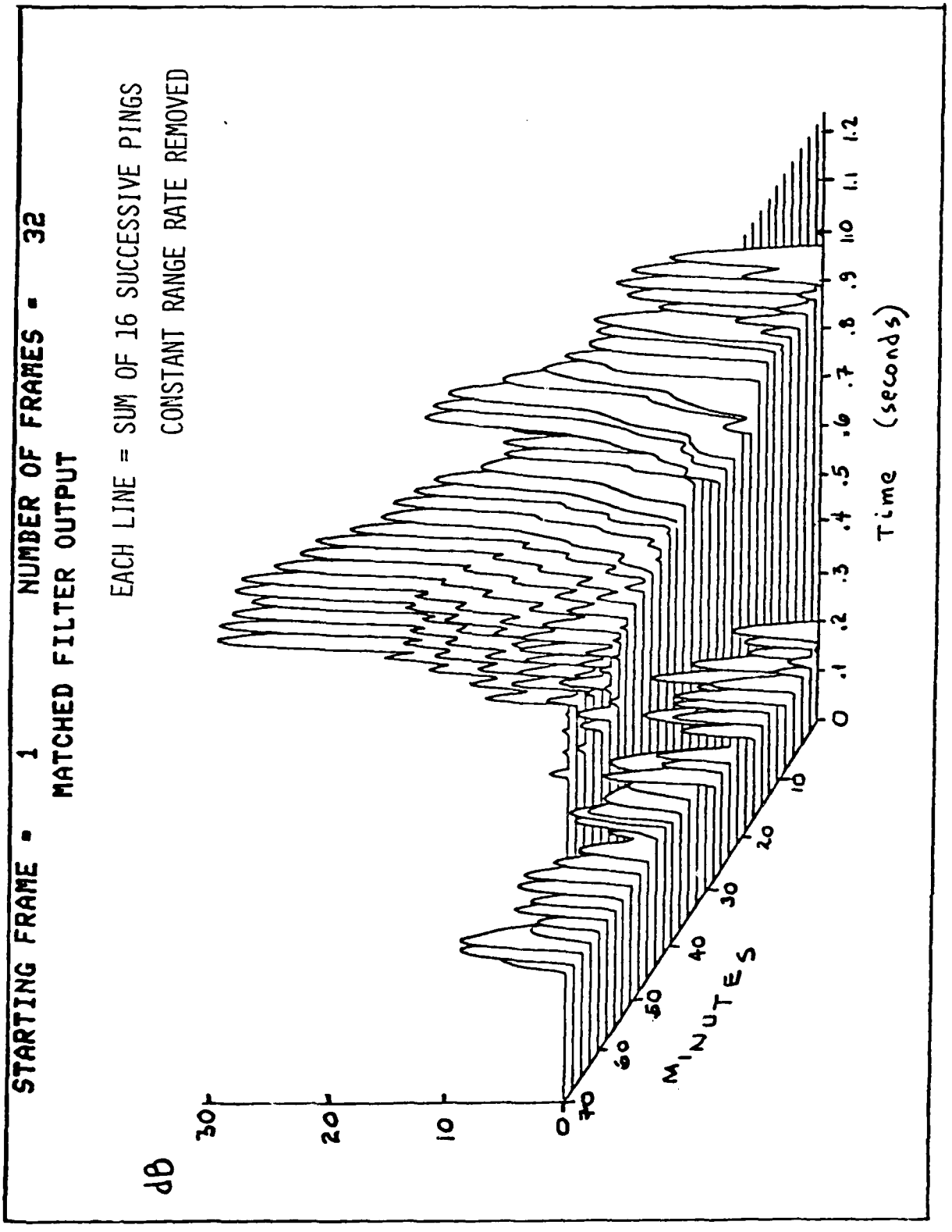

FIG. 14: SIGNAL POWER LEVEL OF AVERAGED PINGS (RANGE VARIES FROM 154 NM, AT FRONT, TO 150 NM)

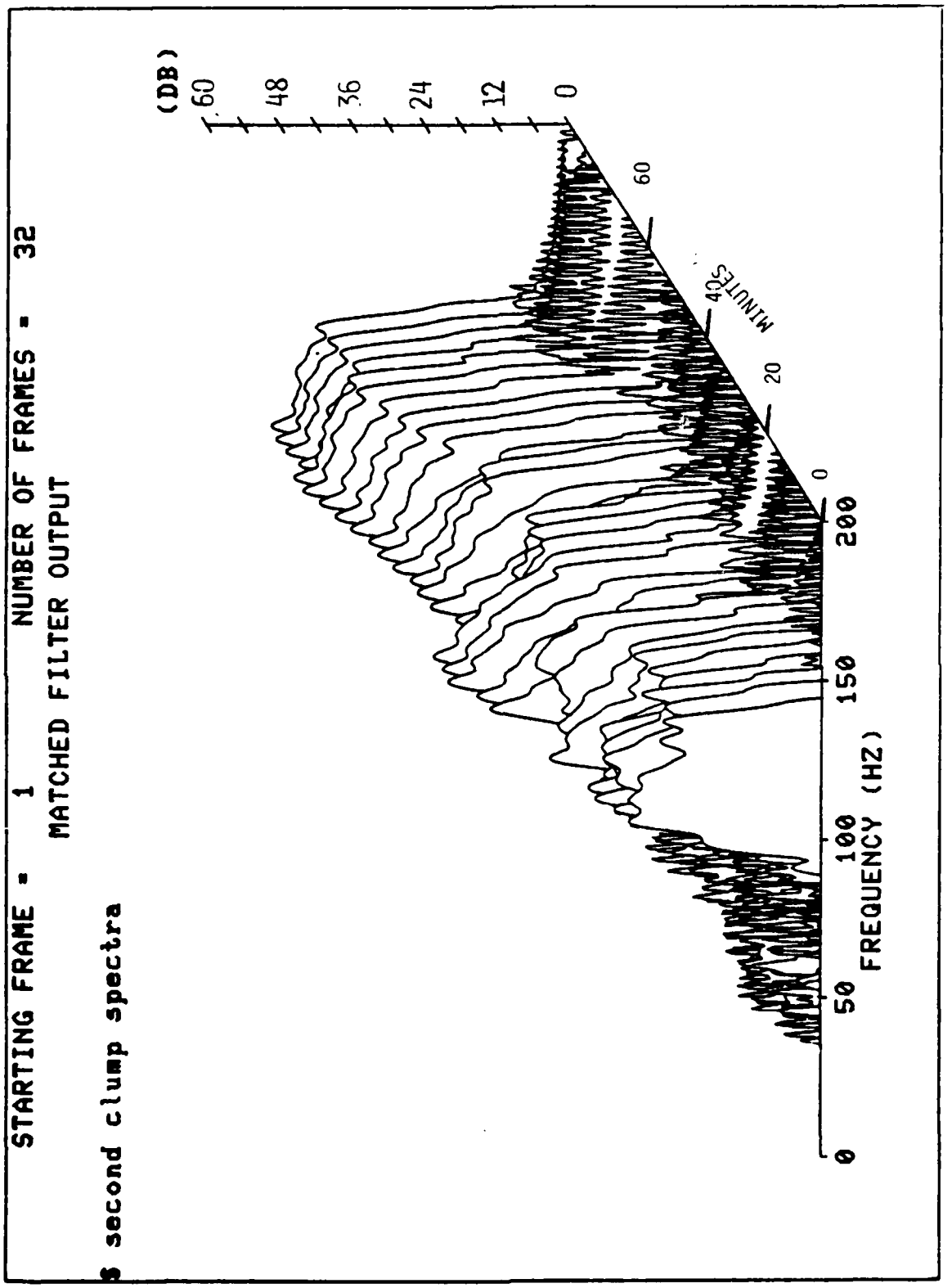

FIG. 15-1: SPECTRUM LEVEL OF THE SECOND CLUSTER OF SIGNAL ENERGY IN AVERAGED PINGS.

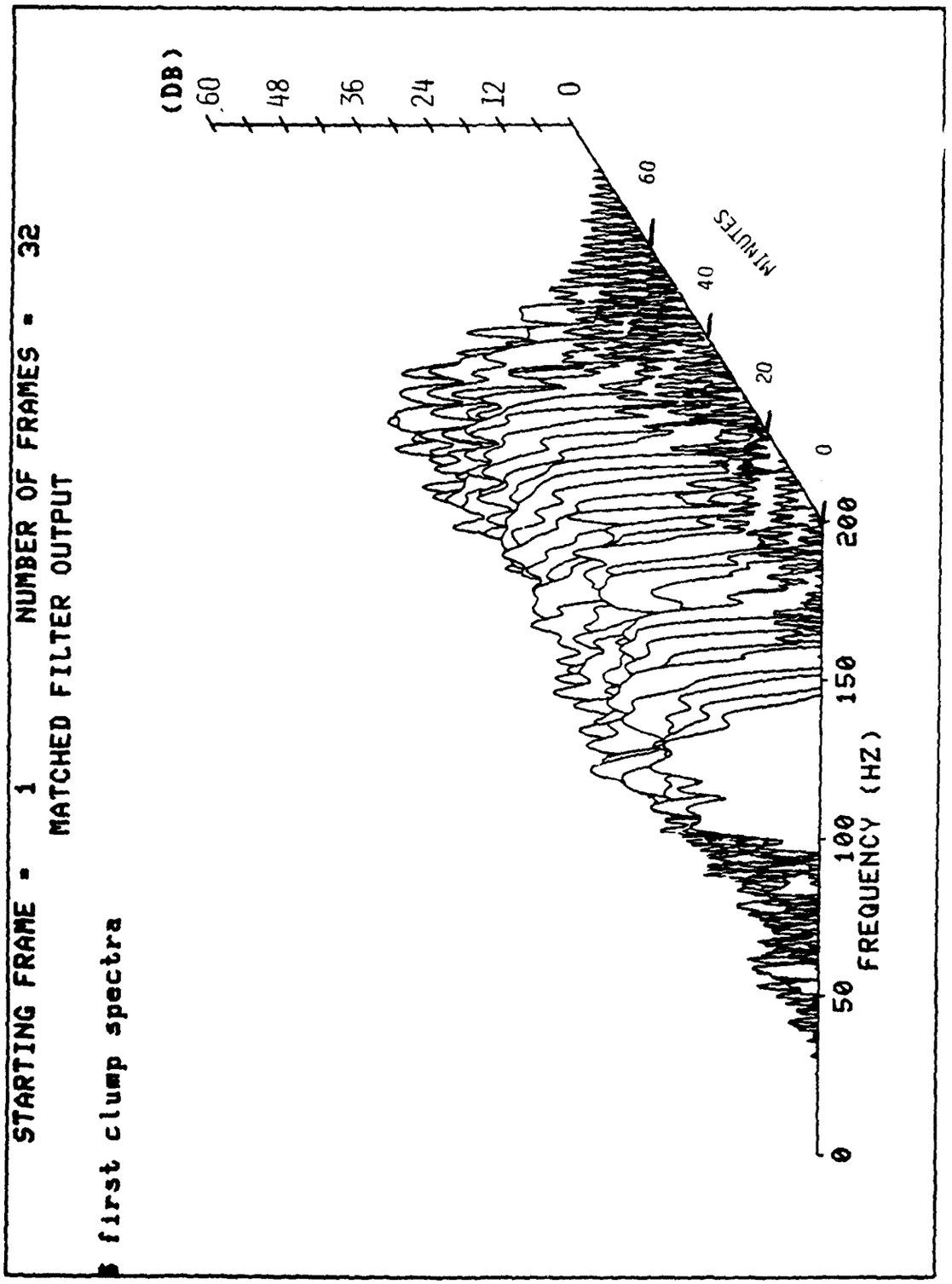

FIG. 15-2: SPECTRUM LEVEL OF THE FIRST CLUSTER OF SIGNAL ENERGY IN AVERAGED PINGS.

that the noise is stationary and Gaussian, the magnitude of the phasor has a Rice distribution with well-known statistical properties [9]. In particular, the squared magnitude I is a random variable with mean value

$$\langle I \rangle = I_s + \langle I_n \rangle$$

where I_s and I_n are the values of I for signal alone and noise alone, respectively. The standard deviation of I is given by

$$\sigma_I = \langle I_n \rangle \ .$$

The ratio of these metrics is easily estimated from previous measurements, reported in Fig. 12:

$$\frac{\langle I_n \rangle}{I_s} = \frac{\text{noise energy/Hz}}{\text{signal energy/Hz}} = \frac{N_0 (0.375)}{E_s/40} \ ,$$

where N_0 is the power spectral density of the noise, the sample window is 0.375 sec long, E_s is the total signal energy, uniformly distributed over a bandwidth of 40 Hz. For the first cluster of signal energy, the data of Fig. 12 indicates that, on average,

$$E_s/N_0 \approx 145,$$

so that the ratio given above equals 0.1. The standard deviation of the measurement is 10% of the mean. The expected frequency-to-frequency variations of the spectrum level, in dB, are about ± 0.5 dB. Since the observed variations are much larger, the hypothesis that they are caused by noise is rejected.

5. DISCUSSION

This analysis of the FM slides from Project DIANA has shown the feasibility in principle of making high-resolution measurements of acoustic transmission characteristics in a conventional 2-ship configuration (towed source, towed array), by means of unconventional signals and signal processing. The particular data at hand could not be used to derive quantitative measures of transmission because of measurement artifacts — especially, the pronounced tilt of the receiving array.

The results of the analysis yield a semi-quantitative confirmation of many of the features predicted from ray theory. The transmitted energy is divided into distinct clusters of arrivals that are easily resolved with signals of moderate bandwidth; their temporal separation drifts slowly with range changes. The very strong arrival associated with transmission near a caustic, or leading edge of a convergence zone, has a very broad frequency response, and small dispersion, so that it is well modeled as a single, ideal path. Other clusters exhibit characteristics associated with a cluster of unresolved paths having a spread in travel time.

The stability of the channel was adequate to allow coherent recombination of successive pings, thereby achieving increased signal-to-noise ratio. Of course, signals of quite different design can be arranged to achieve the same goal. The pertinent parameter here is the range interval (215 m; 17 wavelengths) within which such recombination was undertaken.

Future experiments must use arrays designed to minimize the tilt in order to get good quantitative measurements of the propagation in the ocean. It is also recommended that adaptive beam steering be employed, in order to minimize the distortion of signals that are not incident directly along the main response axis of any preformed beam.

REFERENCES

1. J. E. Barger, *et al.*, "Deep Ocean Test of Active Surveillance System — Project DIANA (U)," BBN Report No. 4282 (January 1980) (CONF.).

2. P. W. Smith, Jr., "Spatial coherence in multipath or multimodal channels," J. Acoust. Soc. Am. 60, 305-310 (1976).

3. W. Jobst and X. Zabalgogeazcoa, "Coherence estimates for signals propagated through acoustic channels with multiple paths," J. Acoust. Soc. Am. 65, 622-630 (1979).

4. P. W. Smith, Jr., "Comments on coherence estimates in multipath channels," J. Acoust. Soc. Am. 67, 1061-1062 (1980).

5. W. R. Hamblen, *et al.*, "Received Signal Characteristics," BBN Tech Memo No. 587 (October, 1980).

6. H. L. Van Trees, *Detection, Estimation, and Modulation Theory* (John Wiley & Sons, New York, 1971), Part III, Chap. 13.

7. C. B. Officer, *Sound Transmission* (McGraw Hill, New York, 1958), Chap. 2.

8. H. Weinberg, "Generic Sonar Model," NUSC Tech. Doc. 5971A, Feb. 1980 The analysis is described in H. Weinberg, "Application of ray theory to acoustic propagation in horizontally stratified oceans," J. Acoust. Soc. Am. 58, 97-109 (1975).

9. For example, see P. Beckmann, *Probability in Communication Engineering* (Harcourt, Brace & World, New York, 1967), Sect. 7.5.

END

DATE
FILMED

1-82

DTIC